Biosurfactant-Stabilized Micropore-Forming GelMA Inks Enable Improved Usability for 3D Printing Applications

Xin-Sheng Qin^{1,‡}, Mian Wang^{1,‡}, Wanlu Li¹, and Yu Shrike Zhang^{1,*}

¹ Division of Engineering in Medicine, Department of Medicine, Brigham and Women's Hospital, Harvard Medical School, Cambridge, MA 02139, USA

[†]These authors contributed equally

^{*}Correspondence address. Division of Engineering in Medicine, Department of Medicine, Brigham and Women's Hospital, Harvard Medical School, Cambridge, MA 02139, USA E-mail: yszhang@research.bwh.harvard.edu

Abstract

Purpose. Three-dimensional (3D) bioprinting offers great potentials in rebuilding tissue mimics through engineering cell-laden constructs. Recently, the unique ability of a new type of micropore-forming bioink developed by us, containing two immiscible aqueous phases of gelatin methacryloyl (GelMA) and poly(ethylene oxide) (PEO), has become attractive since it promotes cellular behaviors. Nevertheless, this initial version of our two-phase aqueous emulsion bioink is generally unstable when experiencing prolonged storage times at room temperature, whereby it will phase-segregate and lose the micropore-forming capacity. This phase-segregation leads to insufficient operational time window for bioprinting, especially for modalities that require a liquid-phase bioink such as digital light processing.

Methods. In this study, we report the development of a set of biosurfactant (rhamnolipids)-stabilized micropore-forming GelMA-based inks, with the goal of significantly enhancing their shelf-lives with enhanced applicability towards 3D printing.

Results. It was observed that the printed constructs using rhamnolipids-stabilized micropore-forming inks, either prepared fresh or stored for hours at room temperature, presented similar microporous structures. In contrast, the micropore-forming inks without biosurfactant-incorporation exhibited severely reduced performances after prolonged storage owing to marked phase-segregation.

Conclusion. Our study suggests that biosurfactant-incorporation enhanced stability of our micropore-forming GelMA inks and therefore, present a wide range of possibilities in further development of two-phase aqueous emulsion inks and bioinks for future 3D printing and bioprinting applications.

Keywords: gelatin methacryloyl; two-phase aqueous emulsion; biosurfactant; (bio)ink; digital light processing; 3D printing

Lay Summary

Three-dimensional (3D) bioprinting offers a collection of enabling technologies to address regenerative engineering and translational medicine problems, by allowing precisely controlled, automated fabrication of volumetric tissue constructs that are both structurally and functionally relevant to their counterparts in the human body. The biomaterials used for bioprinting are of significant importance to ensure proper tissue-production and maturation. We report a micropore-forming ink that is stabilized by biologically derived surfactant, in an effort to promote the stability of the resulting porous structures in 3D-printed architectures, for potential applications in tissue engineering and regenerative medicine.

Introduction

Tissue engineering offers a feasible method for repairing injured or diseased tissues [1, 2]. Recently, this strategy has also been used to fabricate tissue and organ models for drug-screening applications with a possibility of personalization [3-5]. Simulated extracellular microenvironments play an important role in reaching proper biological functions to mimic the target tissues or organs. In particular, the scaffolds, as crucial elements in most tissue-engineering scenarios, facilitate cell attachment, proliferation, and other activities, enabling reproduction of physiologically relevant three-dimensional (3D) microenvironments for tissue-formation [6, 7].

To emulate the extracellular matrix (ECM) in which the cells reside, a variety of (bio)materials have been employed for the construction of tissue-mimicking 3D architectures [8]. Of special interest, hydrogels, a class of highly hydrated polymers, are attractive due to their excellent biocompatible property, as well as readily tunable physicochemical characteristics similar to soft tissues [9, 10]. A number of natural and synthetic hydrogel-forming materials such as collagen, gelatin, alginate, chitosan, hyaluronic acid, and poly(ethylene glycol), have been adopted in the fabrication of hydrogel scaffolds for biological and biomedical applications [11-16]. In most cases, these hydrogels could be fabricated into volumetric functional architectures that imitate *in vivo* microsystems to regulate biological functions [17, 18].

The 3D bioprinting method has emerged as an effective tool to produce tissue mimics by recapitulating the structural complexity of desired tissues [19-23]. In general, 3D bioprinting techniques, such as digital light processing (DLP) and extrusion bioprinting, offer feasibility in patterning bioinks in a spatially well-defined manner to obtain tissue constructs with improved physiological relevancy and reproducibility [24, 25]. Although tremendous progress in bioprinting strategies and bioinks has been made, there is still plenty of room for further improvements. For example, selection of the right biomaterials and cells as the bioinks is of great importance to achieve successful bioprinting [26, 27]. To this end, in many cases it is highly desirable to bioprint hydrogel scaffolds featuring microporous structures, which would allow nutrient- and oxygen-exchanges as well as cell spreading, and thus, enhance cellular functions [28, 29].

Our previous studies have reported a type of micropore-forming bioink based upon two-phase aqueous emulsion of gelatin methacryloyl (GelMA) serving as the continuous phase and poly(ethylene oxide) (PEO) droplets as the porogen [30-33]. Indeed, we demonstrated that this micropore-forming GelMA bioink could be superior to those not inducing micropore-formation,

in terms of supporting cell spreading and proliferation [30-32, 34]. Nevertheless, in this initial formulation, the aqueous two-phase emulsion bioink was unstable with a storage time usually only in the range of tens of minutes, where afterwards the GelMA and the PEO solutions would phase-segregate and reduce the micropore-forming capacity. This limitation becomes a particular problem in DLP-based bioprinting, since the bioinks used in DLP have to remain in the liquid phase during the entirety of the bioprinting procedure, where undesired phase-segregation would be detrimental [24, 35, 36]. There is consequently an urgent need to improve the stability of our micropore-forming aqueous two-phase emulsion bioink for enhanced bioprinting applications.

To overcome this obstacle, green surfactants with low toxicity profiles have been long-used to promote interfacial stability [37, 38]. For instance, rhamnolipids is a metabolic anionic biosurfactant of the glycolipid class, which is produced by *Pseudomonas* or *Burkholderia* [39]. By incorporating this biosurfactant, the advantages of the two-phase aqueous emulsions are further improved with enhanced emulsion stability and prolonged non-phase-segregation period, and as such, the better-retained micropore-formation capacities of the resulting hydrogel constructs [40].

With these in mind, here we propose an efficient approach to stabilize our GelMA/PEO aqueous two-phase emulsion ink formulations by adding rhamnolipids as the biosurfactant (Fig. 1). The concentration effect of rhamnolipids was evaluated, and the performances of the rhamnolipids-stabilized GelMA-PEO emulsions as the micropore-forming inks were assessed in two 3D printing methods including those based on DLP and extrusion. Finally, preliminary cellular analyses were conducted to validate the compatibility of the 3D-printed microporous GelMA constructs.

Materials and Methods

Materials

Gelatin from cold-water fish skin, gelatin from porcine skin, methacrylic anhydride (MA), PEO (molecular weight, $M_w = 300,000$ Da), lithium phenyl-2,4,6-trimethylbenzoylphosphinate (LAP), and 3-(trimethoxysilyl)propyl methacrylate (TMSPMA) were purchased from Sigma-Aldrich (USA). Tris(2,2'-bipyridyl)dichloro-ruthenium(II) hexahydrate with sodium persulfate (Ru/SPS) was purchased from Advanced BioMatrix (USA). was purchased from Penicillin/streptomycin (P/S), phosphate-buffered saline (PBS), Dulbecco's modified Eagle's medium (DMEM), fetal bovine serum (FBS), trypsin-EDTA were obtained from Thermo Fisher

Scientific (USA). Rhamnolipids was purchased from AGAE Technologies (USA). The CellTiter $96^{\text{@}}$ Aqueous One Solution Cell Proliferation Assay kit was obtained from Promega (USA). Syringe filters (0.22 µm) were obtained from VWR International (USA). Dialysis membrane (M_w cut-off = 12-14,000 Da) were purchased from Spectrum Labs (USA).

Synthesis of GelMA

GelMA was synthesized according to our previously published method [31, 33, 41, 42]. 10.0 g of gelatin from cold-water fish skin was dissolved in 100 mL of PBS solution at 50 °C, followed by the addition of 8.0 mL of MA slowly and dropwise with stirring at 500 rpm for 2 h. The reaction was stopped by the addition of 200 mL of PBS. The product was dialyzed for 5 days with dialysis membranes at 40 °C, and ultimately lyophilized using a freeze-dryer. The GelMA derived from fish gelatin was termed as fGelMA. In addition, the GelMA derived from porcine gelatin (termed as pGelMA) also adopted the above method, except that the MA addition amount was 2.0 mL.

Preparation of aqueous two-phase emulsion inks

The formation of GelMA-PEO two-phase emulsion ink was carried out by a modified method from our previous work [30-33]. The 15% w/v fGelMA solution was prepared by dissolving fGelMA in PBS under constant stirring at room temperature. Similarly, 10% w/v pGelMA solution was prepared by dissolving pGelMA in PBS under constant stirring at 37 °C. Rhamnolipids was dissolved in the fGelMA solution or pGelMA solution to reach the final rhamnolipids concentration at 0, 0.5%, 1.0%, 1.5%, or 2.0% w/v. In addition, PEO solution was separately prepared in PBS to reach final concentration at 0.5 %, 1.0 %, or 1.6 % w/v. PEO solution was mixed with the fGelMA solution or the pGelMA solution (v/v = 1/2) by strong vortexing for 10 s, leading to formation of an aqueous two-phase emulsion ink based on fGelMA or pGelMA. The former was intended for DLP printing due to its weaker temperature-sensitivity while the latter was more suitable for extrusion printing [34].

Stability measurements

The stabilities of the fGelMA-PEO micropore-forming inks and the pGelMA-PEO micropore-forming inks were visually evidenced by a fluorescence microscope (Eclipse, Nikon, Japan). Briefly, a droplet of the ink was placed on a glass slide capped by a cover glass at a

predefined time point to prevent evaporation and was observed at room temperature. The distribution of PEO droplet diameters was quantified by the ImageJ software (National Institutes of Health, USA).

DLP printing

To prepare the fGelMA-PEO micropore-forming inks, fresh fGelMA (containing 0 or 1.5% w/v rhamnolipids) and PEO solutions, photoinitiator Ru/SPS (2 mM/20 mM), and photoabsorber Ponceau 4R (2% w/v, Sigma-Aldrich, USA) were mixed to achieve the final formulations [24]. The inks investigated included immediately formed inks and preformed inks that had been stored for 12 h prior to the onset of printing. An in-house-built DLP-based 3D printer was used [17, 32, 43, 44]. For printing of planar patterns, a TMSPMA-coated glass slide with a layer of the micropore-forming ink was exposed under the visible light for 15 s. For 3D printing, cubes (length = 5.83 mm, width = 5.83 mm, height = 7.00 mm) were printed at 15 s for each layer with a 300-µm layer thickness. After printing, the constructs were briefly washed with PBS and imaged under the microscope.

Extrusion printing

Extrusion printing was conducted using an extrusion printer (Allevi 2, 3D Systems, USA) with a digitally controlled pneumatic pressure, as previously reported [45, 46]. The micropore-forming pGelMA-PEO ink was filled into the syringe, followed by cooling at 4 °C and then printed at room temperature. The nozzle moving speed was maintained at 400 mm min⁻¹ under 30 psi. All the emulsion inks (fresh and those stored for 12 h with 0 or 1.5% w/v rhamnolipids) were printed in the presence of 0.2% w/v LAP, and then post-crosslinked *via* UV exposure (10 W cm⁻², 30 s, OmniCure S2000, Excelitas, Canada). The 3D pattern that we designed was a honeycomb lattice structure printed in 1, 4, or 10 layers. After printing, the constructs were briefly washed with PBS and imaged under the microscope.

Cell culture

NIH/3T3 fibroblasts used in this study were purchased from American Type Culture Collection (ATCC, USA) and human umbilical vein endothelial cells (HUVECs) were purchased from Angio-Proteomie (USA). NIH/3T3 fibroblasts were cultured in DMEM supplemented with

10% v/v FBS. HUVECs were cultured in endothelial cell growth medium (EGM-2, Lonza, USA). All the cells were maintained in a humidified incubator with 5% CO₂ at 37 °C (Forma Scientific, USA). The culture medium was exchanged every 2 days.

Cell proliferation assays

A direct contact test between constructs printed with emulsion inks and NIH/3T3 fibroblasts. The printing was performed in an aseptic environment with previously described DLP-based printing process, which can be found in the Section of DLP printing. NIH/3T3 fibroblasts were trypsinized and seeded on the printed samples at a density of 2 × 10 ⁶ cell mL⁻¹. The printed samples were cultured in DMEM containing 10% v/v FBS at 37 °C and 5% CO₂ up to 5 days. At different time points, the 3-(4,5-dimethylthiazol-2-yl)-5-(3-carboxymethoxyphenyl)-2-(4-sulfophenyl)-2H-tetrazolium (MTS) assay was conducted using CellTiter 96[®] AQueous One Solution Cell Proliferation Assay kit. The medium was removed, and the construct was incubated with the assay solution in each well of a 96-well plate for 3 h in dark in the incubator. The absorbance was determined at 490 nm with a spectrophotometer (Molecular Devices, USA).

Hemolysis test

Hemolysis test was performed by a modified method as previously reported [47]. Erythrocytes were used to assess the hemostatic effect of the constructs produced with the micropore-forming fGelMA-PEO ink. The constructs were placed into 1.5-mL Eppendorf tubes and mixed with 5% v/v erythrocyte suspensions (Research Blood Components, USA) diluted with PBS in 37 °C for 1 h. 0.1% v/v Triton X-100 solution was used as the positive control and PBS was used as the negative control. After incubation, erythrocyte suspensions and constructs printed with different formulations were centrifuged at 1,000 rpm for 10 min, and then 100 μL of the supernatant from each tube was added into a well of a 96-well plate. The absorbance of the solution was measured at 540 nm using a spectrophotometer. The hemolysis ratio was calculated as follows:

$$Hemolysis(\%) = (A_p - A_b)/(A_t - A_b)$$

, where A_p is the absorbance value in the experimental group, A_t is the absorbance of the Triton group, and A_b is the absorbance of the PBS group.

Statistical analyses

Data are presented as means \pm standard deviations (SDs). Statistical analyses were conducted in triplicates by two-tailed student's t-test and ANOVA using the SPSS software (version 19.0, IBM Corp., USA). The statistical significance was labeled with *p<0.05.

Results and Discussions

Stability measurements of the GelMA-PEO emulsions

GelMA is a gelatin-based material that has been widely adopted for the fabrication of cell-laden 3D biological tissue constructs, because of its biocompatibility, bioactivity, and tunable mechanical properties [34, 48, 49]. Our previous studies described a novel micropore-forming bioink, prepared by two immiscible aqueous phases of GelMA mixed with PEO [32]. The M_w of PEO was selected at 300,000 Da, since phase-segregation is influenced by the M_w; for instance, low PEO M_w was found to be difficult to form the aqueous two-phase emulation in this system [30-33]. To guarantee the proper physical characteristics of the pore-forming inks, 15% w/v fGelMA was chosen as the base, and PEO at different concentrations (0.5-1.6% w/v) were added at the fGelMA:PEO volume ratio of 2:1. Fig. 2A displays the phase-segregation behaviors of the fGelMA-PEO emulsions after mixing the fGelMA and PEO solutions with vortexing for 10 s. Obvious phase-segregation of the fGelMA-PEO emulsion at 0.5% w/v of PEO was observed to form at approximately 1.5 h; in contrast, at 1.0% w/v PEO and 1.6% w/v PEO, the phase-segregations formed at 1 h and 0.5 h, respectively. The results suggested that the PEO concentration clearly had a negative effect on the emulsion stability in the absence of any biosurfactants, and the phase-segregation was faster when the PEO concentration was higher.

We also quantified the droplet sizes of PEO in the fGelMA-PEO emulsions, which was determined by the PEO concentration as well (Fig. 2B). By randomly measuring 50 single droplets from the optical images, $15.1 \pm 2.2 \,\mu m$ could be observed at 0.5% w/v PEO after the emulsion was immediately created. The droplet size of the fGelMA-PEO emulsion was increased to $65.3 \pm 9.3 \,\mu m$ as the PEO concentration was elevated to 1.6% w/v, while it was in between for the emulsion formed with 1.0% w/v PEO. In all cases, as the phase-segregation started, the PEO droplet sizes became larger and less uniform (Fig. 2C). Nevertheless, the start of change in PEO droplet size did not necessarily indicate the onset of phase-segregation since the latter would usually take longer time to occur. Also of note, the phase-segregation would not be complete; typically, while PEO would relocate as the top part of the ink, the bottom part would still contain certain levels of

emulsions in a formulation-dependent manner, although the diameters of the PEO droplets in this lower portion already would become widely different from their initial sizes. The quantitative measurements were always conducted using the liquid from the lower portions of the inks for all scenarios.

To enhance the stability of the emulsions and gain sufficient operational time window for printing, 1.5% w/v rhamnolipids was added to the micropore-forming fGelMA-PEO inks. As can be observed from Fig. 3A, the existence of rhamnolipids had no major influence on the formation of the emulsion. It was quantified that immediately after emulsion-formation, the droplet size increased from 12.2 ± 1.5 to 41.1 ± 5.4 µm, as the PEO concentration was elevated from 0.5%(w/v) to 1.6% w/v (Fig. 3B). Yet, rhamnolipids significantly increased the storage stability of the fGelMA-PEO emulsion, where remarkable phase-segregation at 0.5% w/v of PEO formed only at approximately 24 h (Fig. 3C), compared to the 1.5 h without the biosurfactant (Fig. 2C). In addition, at 1.0% w/v PEO and 1.6% w/v PEO, phase-segregations did not occur before approximately 12 h and 5 h, respectively, remarkably longer than the 1 h and 0.5 h of time scales when no rhamnolipids was incorporated (Fig. 2C). With the absence of the biosurfactant, the phasesegregation eventually led to larger and less uniform PEO droplets in the micropore-forming inks with different PEO concentrations. For instance, the storage time of the ink with 1.0% w/v of PEO concentration was prolonged from <1 h to 12 h, meanwhile the droplet size increased from 25.4 \pm 6.6 to 42.9 ± 9.8 µm. Of note, the latter size measurement could only be obtained from the lower GelMA-rich portion given the occurrence of phase-segregation. Similar trends were observed in the other two groups as well.

The influence of different rhamnolipids concentrations (0-2.0% w/v) at the same fGelMA/PEO (1.0% w/v) formulation on emulsion storage stability is shown in Fig. 4A. Consistent with previous results, it could be observed that the fGelMA-PEO emulsion without rhamnolipids formed distinct phase-segregation at 0.5 h. However, by adding 0.5%, 1.0 %, 1.5%, or 2% w/v rhamnolipids, the emulsion was held stable for up to 1 h, 5 h, 12 h, or 12 h, respectively. Quantification further indicated that the increased rhamnolipids concentration from 0 to 1.5% w/v resulted in the decrease of droplet sizes of the fGelMA-PEO emulsions from 79.7 \pm 19.3 μ m to 28.6 \pm 5.4 μ m at time 0 h with improved uniformity, yet the droplet size became slightly larger at 36.2 \pm 5.3 μ m when the rhamnolipids concentration was further increased to 2.0% w/v (Fig. 4B).

Moreover, as the rhamnolipids concentration was elevated, the emulsion stability was also monotonically improved, as quantitatively suggested in Fig. 4C.

Synthesizing the observations obtained so far with various parameters studied in the fGelMA-PEO two-phase aqueous emulsions, the fGelMA-PEO formulation consisting of 15% w/v GelMA, 1.0% w/v PEO, and 1.5% w/v rhamnolipids, was employed for subsequent investigations. In addition, we studied the different parameters for their effects on droplet sizes and stability performances of pGelMA-PEO emulsions (Figs. S1-S3, Supporting Information), where similar results to fGelMA could be derived.

3D printing

The micropore-forming fGelMA-PEO ink was employed to evaluate its performance through the DLP method. DLP printing utilizes a layer-by-layer photocrosslinking mechanism [24]. Compare with extrusion printing, DLP printing normally exhibits faster speeds and better resolutions. We first compared the fresh ink and that stored for 12 h at room temperature (Fig. 5A). Without the biosurfactant, the 12-h storage condition led to significant detrimental effects to the aqueous two-phase emulsion in the ink. When we used the bottom portion that contained some remnant emulsions for printing, it only produced vaguely defined patterns that also presented partial loss of the porous structures. Similar results were observed in printed 3D constructs (Fig. 5B). We further showed that the operational window was dramatically prolonged when 1.5% w/v rhamnolipids was added to the fGelMA-PEO ink. It was clear that even after 12 h of storage of the ink, the resulting printed pattern was still as porous as that printed with the same ink freshly made. These results were consistent with those from the morphological observations of the emulsions (Figs. 2-4). Of note, the presence of the biosurfactant did not negatively impact the printability, where both the printed planar and 3D patterns had similar resolutions with those absent of the biosurfactant. Another interesting point that we observed was, the 3D constructs printed with rhamnolipids-stabilized inks, either freshly made or stored for 12 h, seemed to exhibit improved fidelity when compared with the formulation without the biosurfactant (Fig. 5B), possibly also associated with the stabilization effect of rhamnolipids on the PEO droplets during the printing sessions.

Once validated for its printability and stability, rhamnolipids-stabilized fGelMA-PEO ink was utilized to print several different patterns with varying degrees of complexity (Fig. 5C). Our

findings suggested that the use of rhamnolipids might provide a viable solution for increasing the stability of our unique micropore-forming ink achieving a sufficient operational time window for DLP printing, the process of which during a single session can run well-beyond 0.5 h, the critical time of phase-segregation if no biosurfactant is incorporated.

In addition, the micropore-forming pGelMA-PEO ink was also evaluated using extrusion printing. As can be seen from Fig. 6, single- or multi-layered honeycomb structures could be readily printed and post-crosslinked by UV. Top views of these same structures are illustrated in Fig. S4. The printed constructs using the rhamnolipids-stabilized ink both fresh and stored for 12 h exhibited integral structures. In contrast, constructs produced with the ink in the absence of the biosurfactant indicated slightly reduced integrity, especially for that stored for 12 h likely due to significant phase-segregation. Therefore, the performance of the pGelMA-PEO micropore-forming ink could be as well-improved through stabilization with the biosurfactant rhamnolipids, although this effect might not be as obvious as in DLP printing given the need for pre-cooling prior to extrusion printing [50].

Biocompatibility evaluation

Good biocompatibility plays an essential role in the development of inks and bioinks. Considering that enhancing the emulsion stability of the fGelMA-PEO ink is of particular interest in DLP-based printing, only fGelMA-PEO inks were evaluated here. A direct-contact test between NIH/3T3 fibroblasts and 3D-printed constructs with different ink formulations was carried out. As shown in Fig. 7A, the viabilities of the NIH/3T3 fibroblasts cultured on the scaffolds formed with the fGelMA-PEO ink and the rhamnolipids-stabilized fGelMA-PEO ink were similar across the 5-day culture period. The morphologies of HUVECs in Fig. 7B were consistent with the quantitative results. The cell spreading on constructs printed with different formulations exhibited excellent cell attachment, suggesting that the existence of rhamnolipids had no significant toxicity to the cells.

To further evaluate the hemocompatibility of these printed constructs, *in vitro* hemolysis test was performed. The photograph in Fig. 7C presented the obvious difference in color between positive control (0.1% v/v Triton X-100), negative control (PBS), and three printed groups. Contrary to the bright red color in the Triton X-100 group, all three printed groups were observed to be near-transparent, similar to the negative control (PBS). As the quantitative data shown in Fig.

7D, the construct formed by the rhamnolipids-stabilized fGelMA-PEO ink exhibited a low hemolysis ratio (0.47%), which was close to the negative control (0.46%), as well as the constructs printed with fGelMA (0.45%) and fGelMA-PEO (0.51%) inks. On the basis of these results, we concluded that the cytocompatibility/hemocompatibility of the hydrogel constructs printed from the rhamnolipids-stabilized fGelMA-PEO ink were as good as of those made from fGelMA-PEO ink without biosurfactant, enabling a wide range of possibilities for applications in 3D printing.

Conclusions

In conclusion, we have described a class of biosurfactant-stabilized GelMA/PEO aqueous two-phase emulsion inks with improved stability and printability. The rhamnolipids concentrations were investigated for stable emulsion-formulation and enhanced storage time. The optimized rhamnolipids-stabilized GelMA-PEO emulsions as the micropore-forming inks were further evaluated by two bioprinting methods including DLP and extrusion. By containing rhamnolipids, the stabilized GelMA-PEO inks showed excellent printability in both printing methods, especially for those stored for 12 h compared with the ink without biosurfactant. Additionally, constructs printed with different formulations exhibited good cell adhesion and excellent biocompatibility. Collectively, our results demonstrated that the biosurfactant-stabilized GelMA-PEO inks may shed new light on employing these unique micropore-forming inks for widespread 3D printing and biomedical applications. Nevertheless, in-depth cellular studies are still required in the future to further demonstrate the biological performances of our rhamnolipids-stabilized micropore-forming inks. Moreover, extending the biosurfactant-stabilized micropore-forming inks into bioinks by incorporating cells may require additional optimizations as well.

Declarations

Funding. The authors gratefully acknowledge funding from the National Institutes of Health (R21EB025270, R21EB026175), the National Science Foundation (NSF-CBET-1936105), and the Brigham Research Institute.

Conflicts of interest/Competing interests. None.

Availability of data and material. The datasets that support the findings of this study are available from the corresponding authors upon reasonable request. All requests for raw and analyzed data and materials will be promptly reviewed by the Brigham and Women's Hospital and

Utrecht University to verify whether the request is subject to any intellectual property or confidentiality obligations. Any data and materials that can be shared will be released via a Material Transfer Agreement.

Code availability. Not applicable.

Ethics approval. Not applicable.

Consent to participate. All authors consent to participate.

Consent for publication. All authors consent for publication.

References

- [1] S.S. Kim, S. Kaihara, M.S. Benvenuto, R.S. Choi, B.S. Kim, D.J. Mooney, G.A. Taylor, J.P. Vacanti, Regenerative signals for intestinal epithelial organoid units transplanted on biodegradable polymer scaffolds for tissue engineering of small intestine, Transplantation 67(2) (1999) 227-33.
- [2] A. Atala, F.K. Kasper, A.G. Mikos, Engineering complex tissues, Sci Transl Med 4(160) (2012) 160rv12.
- [3] A. Khademhosseini, R. Langer, A decade of progress in tissue engineering, Nat Protoc 11(10) (2016) 1775-81.
- [4] X. Ma, J. Liu, W. Zhu, M. Tang, N. Lawrence, C. Yu, M. Gou, S. Chen, 3D bioprinting of functional tissue models for personalized drug screening and in vitro disease modeling, Adv Drug Deliv Rev 132 (2018) 235-251.
- [5] L. Moroni, J.A. Burdick, C. Highley, S.J. Lee, Y. Morimoto, S. Takeuchi, J.J. Yoo, Biofabrication strategies for 3D in vitro models and regenerative medicine, Nat Rev Mater 3(5) (2018) 21-37.
- [6] F.M. Chen, X. Liu, Advancing biomaterials of human origin for tissue engineering, Prog Polym Sci 53 (2016) 86-168.
- [7] E.S. Place, N.D. Evans, M.M. Stevens, Complexity in biomaterials for tissue engineering, Nat Mater 8(6) (2009) 457-70.
- [8] G.S. Hussey, J.L. Dziki, S.F. Badylak, Extracellular matrix-based materials for regenerative medicine, Nature Reviews Materials 3(7) (2018) 159-173.
- [9] Y.S. Zhang, A. Khademhosseini, Advances in engineering hydrogels, Science 356(6337) (2017).
- [10] J.L. Drury, D.J. Mooney, Hydrogels for tissue engineering: scaffold design variables and applications, Biomaterials 24(24) (2003) 4337-51.
- [11] N. Huebsch, E. Lippens, K. Lee, M. Mehta, S.T. Koshy, M.C. Darnell, R.M. Desai, C.M. Madl, M. Xu, X. Zhao, O. Chaudhuri, C. Verbeke, W.S. Kim, K. Alim, A. Mammoto, D.E. Ingber, G.N. Duda, D.J. Mooney, Matrix elasticity of void-forming hydrogels controls transplanted-stem-cell-mediated bone formation, Nat Mater 14(12) (2015) 1269-77.

- [12] K. Yue, G. Trujillo-de Santiago, M.M. Alvarez, A. Tamayol, N. Annabi, A. Khademhosseini, Synthesis, properties, and biomedical applications of gelatin methacryloyl (GelMA) hydrogels, Biomaterials 73 (2015) 254-71.
- [13] F. Zhou, Y. Hong, R. Liang, X. Zhang, Y. Liao, D. Jiang, J. Zhang, Z. Sheng, C. Xie, Z. Peng, X. Zhuang, V. Bunpetch, Y. Zou, W. Huang, Q. Zhang, E.V. Alakpa, S. Zhang, H. Ouyang, Rapid printing of bio-inspired 3D tissue constructs for skin regeneration, Biomaterials 258 (2020) 120287.
- [14] Y.-H. Tsou, J. Khoneisser, P.-C. Huang, X. Xu, Hydrogel as a bioactive material to regulate stem cell fate, Bioactive materials 1(1) (2016) 39-55.
- [15] X. Zheng Shu, Y. Liu, F.S. Palumbo, Y. Luo, G.D. Prestwich, In situ crosslinkable hyaluronan hydrogels for tissue engineering, Biomaterials 25(7-8) (2004) 1339-48.
- [16] Z. Li, H.R. Ramay, K.D. Hauch, D. Xiao, M. Zhang, Chitosan-alginate hybrid scaffolds for bone tissue engineering, Biomaterials 26(18) (2005) 3919-28.
- [17] A.K. Miri, D. Nieto, L. Iglesias, H. Goodarzi Hosseinabadi, S. Maharjan, G.U. Ruiz-Esparza, P. Khoshakhlagh, A. Manbachi, M.R. Dokmeci, S. Chen, S.R. Shin, Y.S. Zhang, A. Khademhosseini, Microfluidics-Enabled Multimaterial Maskless Stereolithographic Bioprinting, Adv Mater 30(27) (2018) e1800242.
- [18] K.Y. Lee, D.J. Mooney, Hydrogels for tissue engineering, Chemical reviews 101(7) (2001) 1869-1880.
- [19] Y.S. Zhang, K. Yue, J. Aleman, K.M. Moghaddam, S.M. Bakht, J. Yang, W. Jia, V. Dell'Erba, P. Assawes, S.R. Shin, M.R. Dokmeci, R. Oklu, A. Khademhosseini, 3D Bioprinting for Tissue and Organ Fabrication, Ann Biomed Eng 45(1) (2017) 148-163.
- [20] S.V. Murphy, P. De Coppi, A. Atala, Opportunities and challenges of translational 3D bioprinting, Nat Biomed Eng 4(4) (2020) 370-380.
- [21] R. Levato, T. Jungst, R.G. Scheuring, T. Blunk, J. Groll, J. Malda, From Shape to Function: The Next Step in Bioprinting, Adv Mater 32(12) (2020) e1906423.
- [22] L. Moroni, T. Boland, J.A. Burdick, C. De Maria, B. Derby, G. Forgacs, J. Groll, Q. Li, J. Malda, V.A. Mironov, C. Mota, M. Nakamura, W. Shu, S. Takeuchi, T.B.F. Woodfield, T. Xu, J.J. Yoo, G. Vozzi, Biofabrication: A Guide to Technology and Terminology, Trends Biotechnol. 36(4) (2018) 384-402.
- [23] J.M. Lee, S.L. Sing, M. Zhou, W.Y. Yeong, 3D bioprinting processes: A perspective on classification and terminology, International journal of bioprinting 4(2) (2018) 151-151.
- [24] W. Li, L.S. Mille, J.A. Robledo, T. Uribe, V. Huerta, Y.S. Zhang, Recent Advances in Formulating and Processing Biomaterial Inks for Vat Polymerization-Based 3D Printing, Adv Healthc Mater 9(15) (2020) e2000156.
- [25] X. Cui, J. Li, Y. Hartanto, M. Durham, J. Tang, H. Zhang, G. Hooper, K. Lim, T. Woodfield, Advances in Extrusion 3D Bioprinting: A Focus on Multicomponent Hydrogel-Based Bioinks, Adv Healthc Mater 9(15) (2020) e1901648.

- [26] S. Vanaei, M.S. Parizi, S. Vanaei, F. Salemizadehparizi, H.R. Vanaei, An Overview on Materials and Techniques in 3D Bioprinting Toward Biomedical Application, Engineered Regeneration 2 (2021) 1-18.
- [27] Y.S. Zhang, G. Haghiashtiani, T. Hübscher, D.J. Kelly, J.M. Lee, M. Lutolf, M.C. McAlpine, W.Y. Yeong, M. Zenobi-Wong, J. Malda, 3D extrusion bioprinting methods, Nature Reviews Methods Primers 1(1) (2021) 75.
- [28] R.D. Pedde, B. Mirani, A. Navaei, T. Styan, S. Wong, M. Mehrali, A. Thakur, N.K. Mohtaram, A. Bayati, A. Dolatshahi-Pirouz, M. Nikkhah, S.M. Willerth, M. Akbari, Emerging Biofabrication Strategies for Engineering Complex Tissue Constructs, Adv Mater 29(19) (2017).
- [29] G. Bao, T. Jiang, H. Ravanbakhsh, A. Reyes, Z. Ma, M. Strong, H. Wang, J.M. Kinsella, J. Li, L. Mongeau, Triggered micropore-forming bioprinting of porous viscoelastic hydrogels, Mater Horiz 7(9) (2020) 2336-2347.
- [30] G. Ying, J. Manriquez, D. Wu, J. Zhang, N. Jiang, S. Maharjan, D.H. Hernandez Medina, Y.S. Zhang, An open-source handheld extruder loaded with pore-forming bioink for in situ wound dressing, Mater Today Bio 8 (2020) 100074.
- [31] G. Ying, N. Jiang, C. Parra, G. Tang, J. Zhang, H. Wang, S. Chen, N.P. Huang, J. Xie, Y.S. Zhang, Bioprinted Injectable Hierarchically Porous Gelatin Methacryloyl Hydrogel Constructs with Shape-Memory Properties, Adv Funct Mater 30(46) (2020).
- [32] G.L. Ying, N. Jiang, S. Maharjan, Y.X. Yin, R.R. Chai, X. Cao, J.Z. Yang, A.K. Miri, S. Hassan, Y.S. Zhang, Aqueous Two-Phase Emulsion Bioink-Enabled 3D Bioprinting of Porous Hydrogels, Adv Mater 30(50) (2018) e1805460.
- [33] R. Levato, K.S. Lim, W. Li, A.U. Asua, L.B. Peña, M. Wang, M. Falandt, P.N. Bernal, D. Gawlitta, Y.S. Zhang, T.B.F. Woodfield, J. Malda, High-resolution lithographic biofabrication of hydrogels with complex microchannels from low-temperature-soluble gelatin bioresins, Materials Today Bio 12 (2021) 100162.
- [34] G. Ying, N. Jiang, C. Yu, Y.S. Zhang, Three-dimensional bioprinting of gelatin methacryloyl (GelMA), Bio-Design and Manufacturing 1(4) (2018) 215-224.
- [35] C. Yu, J. Schimelman, P. Wang, K.L. Miller, X. Ma, S. You, J. Guan, B. Sun, W. Zhu, S. Chen, Photopolymerizable Biomaterials and Light-Based 3D Printing Strategies for Biomedical Applications, Chem Rev 120(19) (2020) 10695-10743.
- [36] M. Lee, R. Rizzo, F. Surman, M. Zenobi-Wong, Guiding Lights: Tissue Bioprinting Using Photoactivated Materials, Chem. Rev. 120(19) (2020) 10950-11027.
- [37] C.B.B. Farias, F.C. Almeida, I.A. Silva, T.C. Souza, H.M. Meira, F. Rita de Cássia, J.M. Luna, V.A. Santos, A. Converti, I.M. Banat, Production of green surfactants: market prospects, Electronic Journal of Biotechnology (2021).
- [38] E. Turos, J.C. Garay-Jimenez, A.J. Sona, An evaluation of non-ionic surfactants on the cytotoxicity and activity of poly (butyl acrylate/styrene) nanoparticle emulsions, Journal of Nanoparticle Research 21(7) (2019) 1-8.

- [39] A.M. Abdel-Mawgoud, F. Lepine, E. Deziel, Rhamnolipids: diversity of structures, microbial origins and roles, Appl Microbiol Biotechnol 86(5) (2010) 1323-36.
- [40] A. Schmid, A. Kollmer, B. Witholt, Effects of biosurfactant and emulsification on two-liquid phase Pseudomonas oleovorans cultures and cell-free emulsions containing n-decane, Enzyme and microbial technology 22(6) (1998) 487-493.
- [41] S. Maharjan, J. Alva, C. Cámara, A.G. Rubio, D. Hernández, C. Delavaux, E. Correa, M.D. Romo, D. Bonilla, M.L. Santiago, Symbiotic photosynthetic oxygenation within 3D-bioprinted vascularized tissues, Matter 4(1) (2021) 217-240.
- [42] J. Gong, C.C.L. Schuurmans, A.M.V. Genderen, X. Cao, W. Li, F. Cheng, J.J. He, A. Lopez, V. Huerta, J. Manriquez, R. Li, H. Li, C. Delavaux, S. Sebastian, P.E. Capendale, H. Wang, J. Xie, M. Yu, R. Masereeuw, T. Vermonden, Y.S. Zhang, Complexation-induced resolution enhancement of 3D-printed hydrogel constructs, Nat Commun 11(1) (2020) 1267.
- [43] W. Li, M. Wang, L.S. Mille, J.A. Robledo, V. Huerta, T. Uribe, F. Cheng, H. Li, J. Gong, T. Ching, C.A. Murphy, A. Lesha, S. Hassan, T.B.F. Woodfield, K.S. Lim, Y.S. Zhang, A Smartphone-Enabled Portable Digital Light Processing 3D Printer, Adv. Mater. 33(35) (2021) 2102153.
- [44] M. Wang, W. Li, L.S. Mille, T. Ching, Z. Luo, G. Tang, C.E. Garciamendez, A. Lesha, M. Hashimoto, Y.S. Zhang, Digital Light Processing Based Bioprinting with Composable Gradients, Adv. Mater. n/a(n/a) (2021) 2107038.
- [45] H. Li, F. Cheng, W. Li, X. Cao, Z. Wang, M. Wang, J.A. Robledo-Lara, J. Liao, C. Chavez-Madero, S. Hassan, J. Xie, G. Trujillo-de Santiago, M.M. Alvarez, J. He, Y.S. Zhang, Expanding sacrificially printed microfluidic channel-embedded paper devices for construction of volumetric tissue models in vitro, Biofabrication 12(4) (2020) 045027.
- [46] F. Cheng, X. Cao, H. Li, T. Liu, X. Xie, D. Huang, S. Maharjan, H.P. Bei, A. Gómez, J. Li, Generation of cost-effective paper-based tissue models through matrix-assisted sacrificial 3d printing, Nano letters 19(6) (2019) 3603-3611.
- [47] Y. Liang, X. Zhao, T. Hu, B. Chen, Z. Yin, P.X. Ma, B. Guo, Adhesive Hemostatic Conducting Injectable Composite Hydrogels with Sustained Drug Release and Photothermal Antibacterial Activity to Promote Full-Thickness Skin Regeneration During Wound Healing, Small 15(12) (2019) e1900046.
- [48] F. Fu, L. Shang, Z. Chen, Y. Yu, Y. Zhao, Bioinspired living structural color hydrogels, Science Robotics 3(16) (2018) eaar8580.
- [49] F. Fu, Z. Chen, Z. Zhao, H. Wang, L. Shang, Z. Gu, Y. Zhao, Bio-inspired self-healing structural color hydrogel, Proct. Natl. Acad. Sci. U.S.A. 114(23) (2017) 5900.
- [50] W. Liu, M.A. Heinrich, Y. Zhou, A. Akpek, N. Hu, X. Liu, X. Guan, Z. Zhong, X. Jin, A. Khademhosseini, Y.S. Zhang, Extrusion Bioprinting of Shear-Thinning Gelatin Methacryloyl Bioinks, Adv Healthc Mater 6(12) (2017).

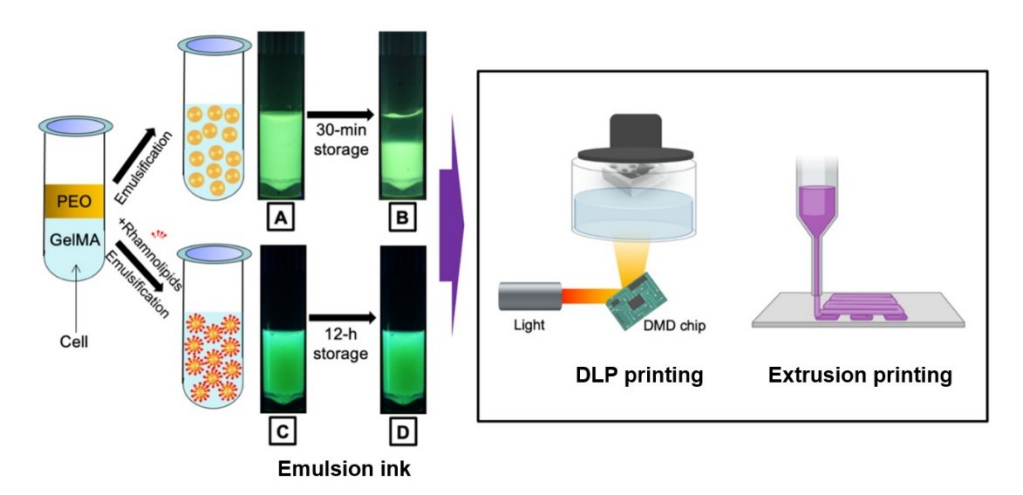


Figure 1. Schematics showing the formulation of GelMA-PEO two-phase aqueous emulsion and rhamnolipids-stabilized GelMA-PEO micropore-forming inks, as well as their applications for DLP and extrusion printing.

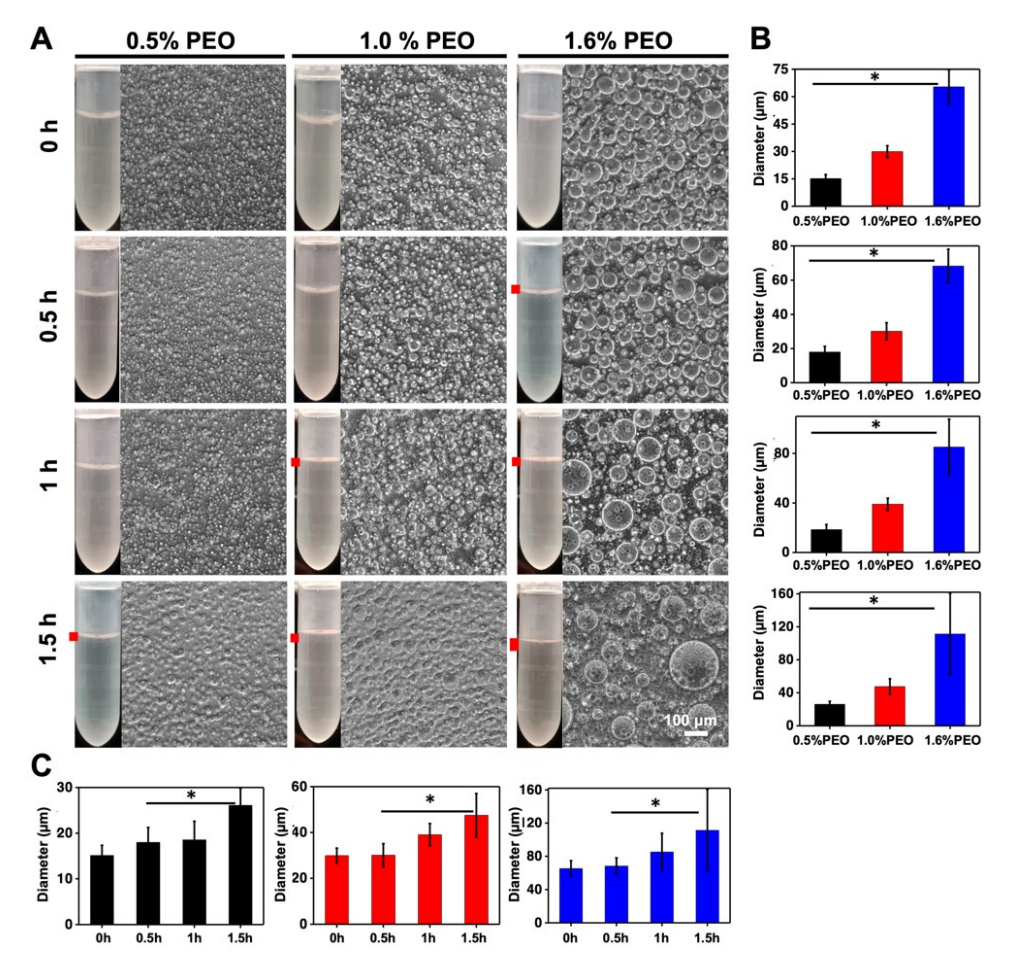


Figure 2. Characterizations of the fGelMA-PEO micropore-forming inks. (A) Optical micrographs showing the fGelMA-PEO inks with different PEO concentrations (0.5, 1.0, 1.6% w/v) and different storage times (0-1.5 h) at room temperature. Red bars indicate the phase-segregation heights of the emulsions in the inks over time. (B) Quantification showing the average sizes of the PEO emulsion droplets of the fGelMA-PEO inks at each time point as a function of different PEO concentrations (0.5, 1.0, 1.6% w/v). (C) Quantification showing the average sizes of the PEO emulsion droplets of the fGelMA-PEO inks at each PEO concentration as a function of different storage times (0-1.5 h) at room temperature.

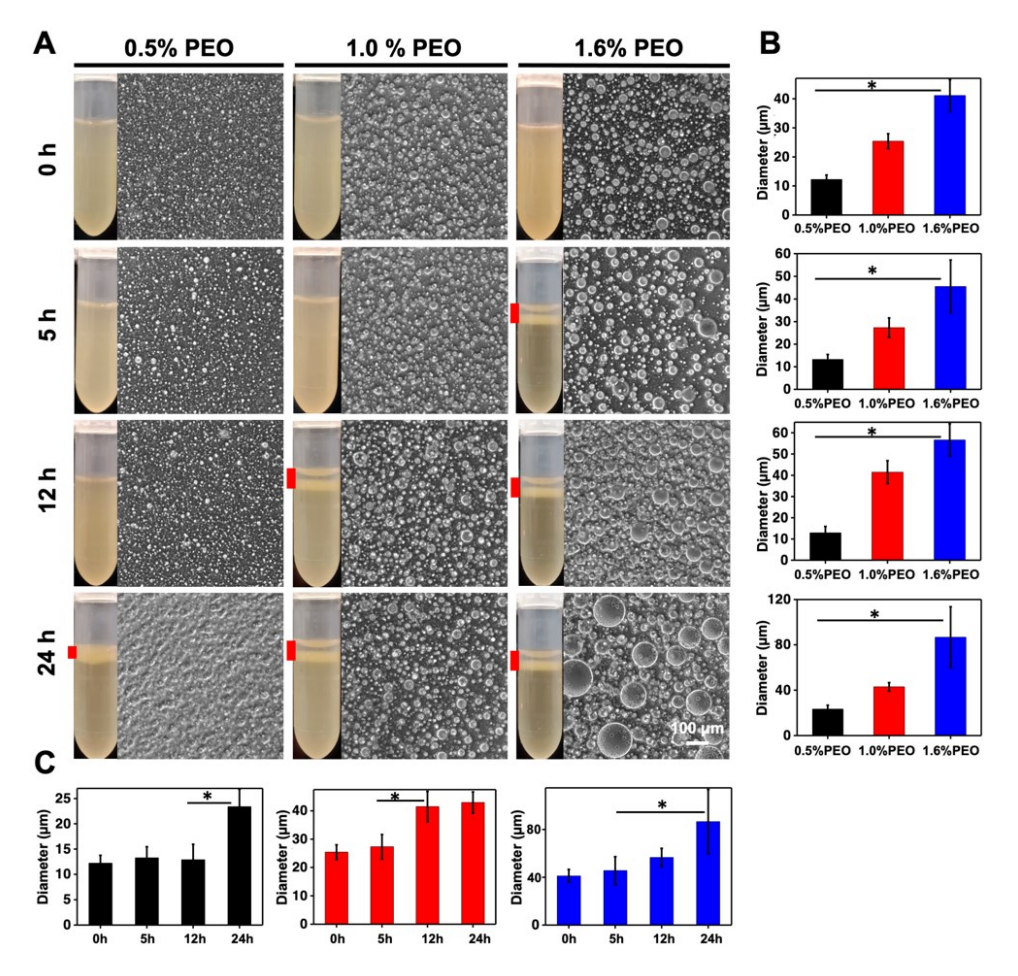


Figure 3. Characterizations of the fGelMA-PEO micropore-forming inks with 1.5% w/v rhamnolipids. (A) Optical micrographs showing the rhamnolipids-stabilized fGelMA-PEO inks with different PEO concentrations (0.5, 1.0, and 1.6% w/v) and different storage times (0-24 h) at room temperature. Red bars indicate the phase-segregation heights of the emulsions in the inks over time. (B) Quantification showing the average sizes of the PEO emulsion droplets of rhamnolipids-stabilized fGelMA-PEO inks with different PEO concentrations (0.5, 1.0, and 1.6% w/v). (C) Quantification showing the average sizes of the PEO emulsion droplets of the rhamnolipids-stabilized fGelMA-PEO inks at each PEO concentration as a function of different storage times (0-24 h) at room temperature.

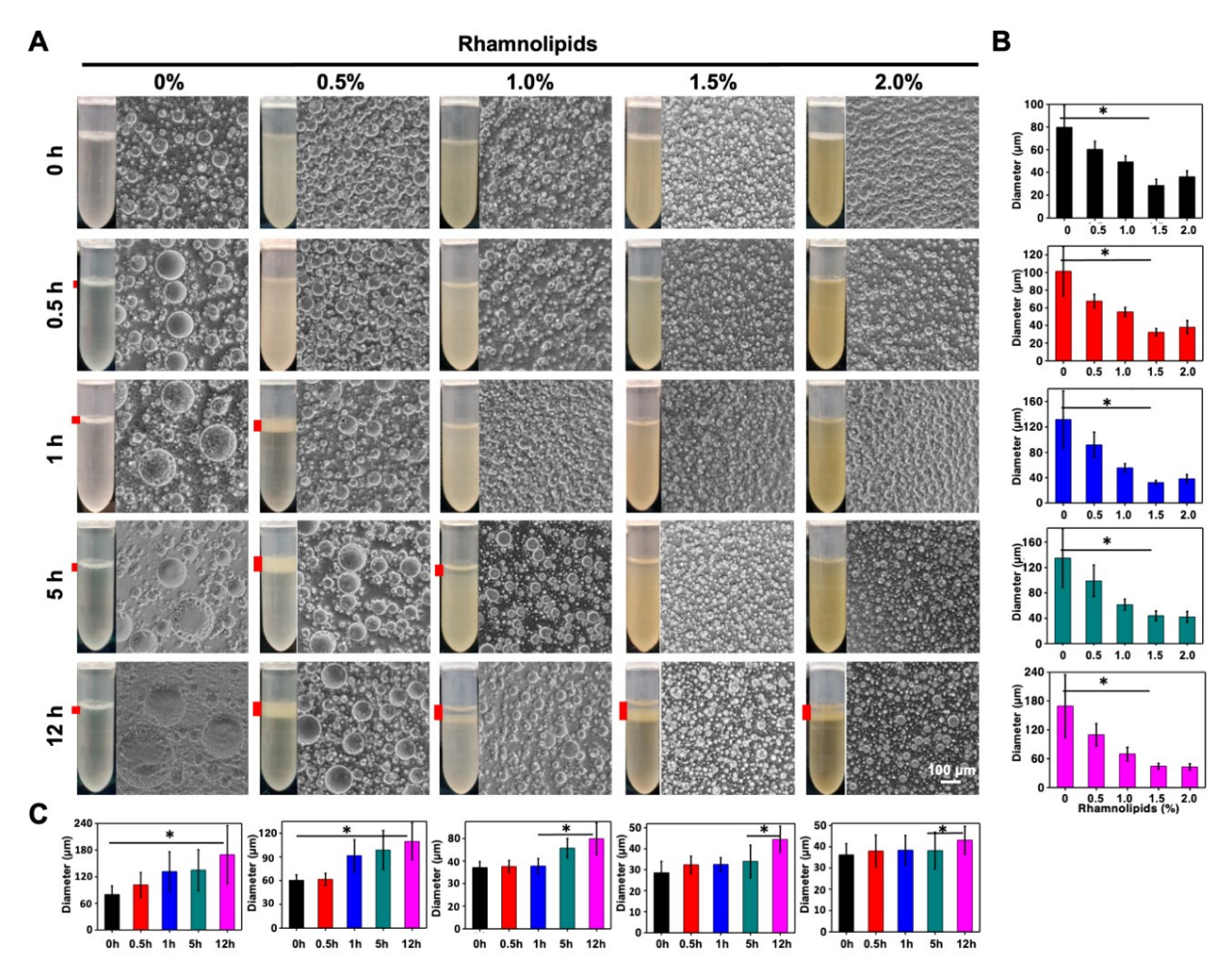


Figure 4. The influence of rhamnolipids concentrations on the fGelMA-PEO micropore-forming ink-formation and stabilization. (A) Optical micrographs showing fGelMA-PEO inks at 1.0% w/v PEO concentration with different rhamnolipids concentrations (0, 0.5, 1.0, 1.5, and 2.0% w/v) and different storage times (0-12 h) at room temperature. Red bars indicate the phase-segregation heights of the emulsions in the inks over time. (B) Quantification showing the average sizes of the PEO emulsion droplets of the fGelMA-PEO inks at 1.0% w/v PEO concentration with different rhamnolipids concentrations (0, 0.5, 1.0, 1.5, and 2.0% w/v). (C) Quantification showing the average sizes of the PEO emulsion droplets of the rhamnolipids-stabilized fGelMA-PEO inks at each rhamnolipids concentration as a function of different storage times (0-12 h) at room temperature.

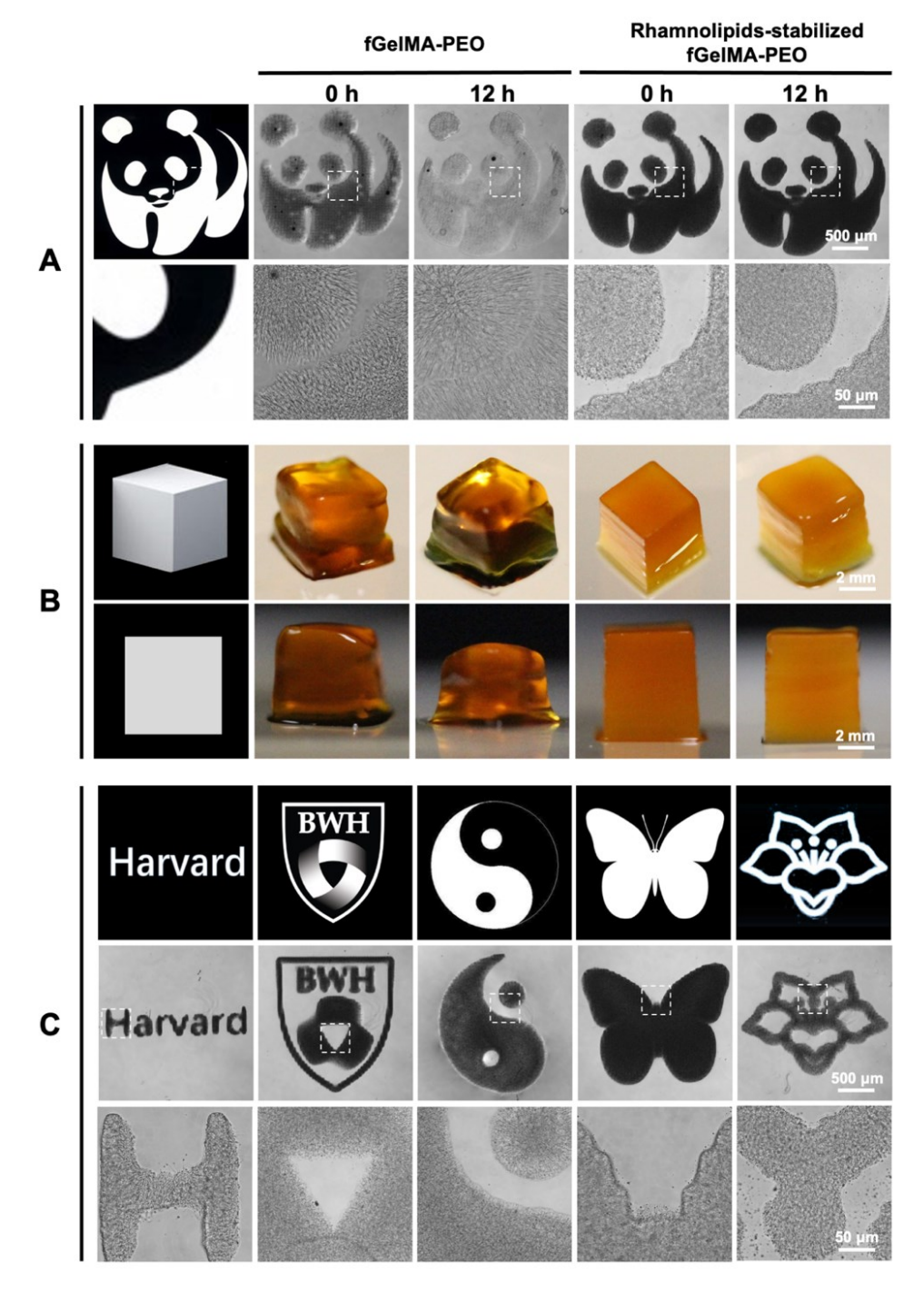


Figure 5. DLP printing of the fGelMA-PEO micropore-forming inks. (A) Designed pattern, photographs, and micrographs of printed 2D constructs of the fGelMA-PEO and rhamnolipids-stabilized fGelMA-PEO inks as a function of different storage times (0 and 12 h) at room temperature. (B) Designed pattern and photographs of corresponding 3D constructs printed from the fGelMA-PEO and rhamnolipids-stabilized fGelMA-PEO inks as a function of different storage times (0 and 12 h) at room temperature. (C) Different designed patterns and photographs of

corresponding constructs printed from the rhamnolipids-stabilized fGelMA-PEO inks at low magnification (2^{\times}) and high magnification (20^{\times}) at 12 h or storage at room temperature.

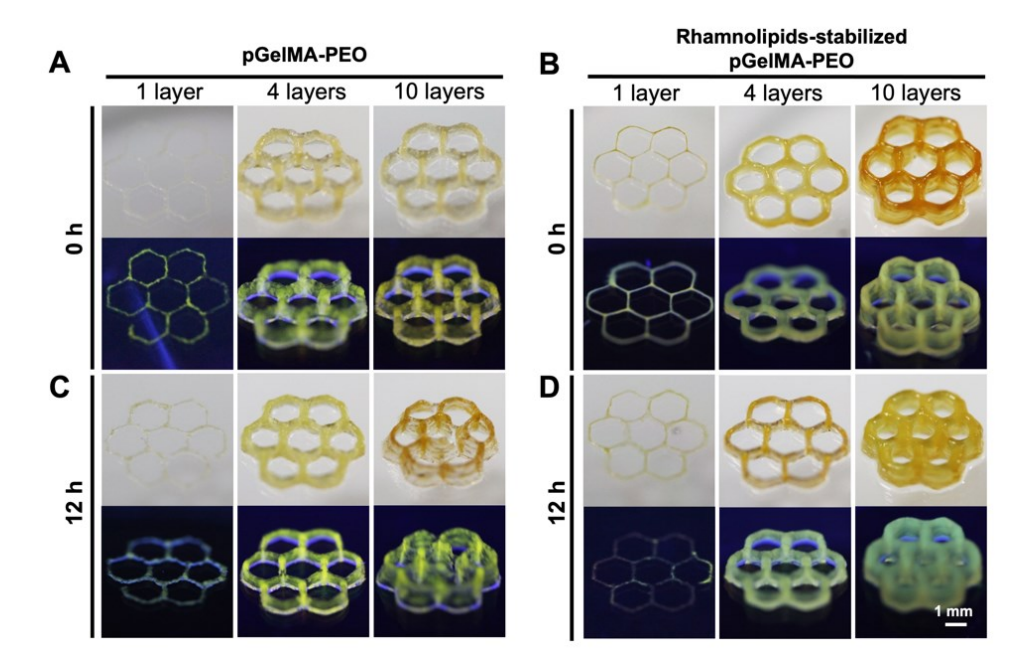


Figure 6. Extrusion printing of the pGelMA-PEO micropore-forming inks. Regular and fluorescence photographs showing oblique views of 3D constructs printed from (A) fresh pGelMA-PEO ink and (B) rhamnolipids-stabilized pGelMA-PEO ink, as well as (C, D) 3D constructs printed with the same formulations stored at room temperature for 12 h, all under oblique view.

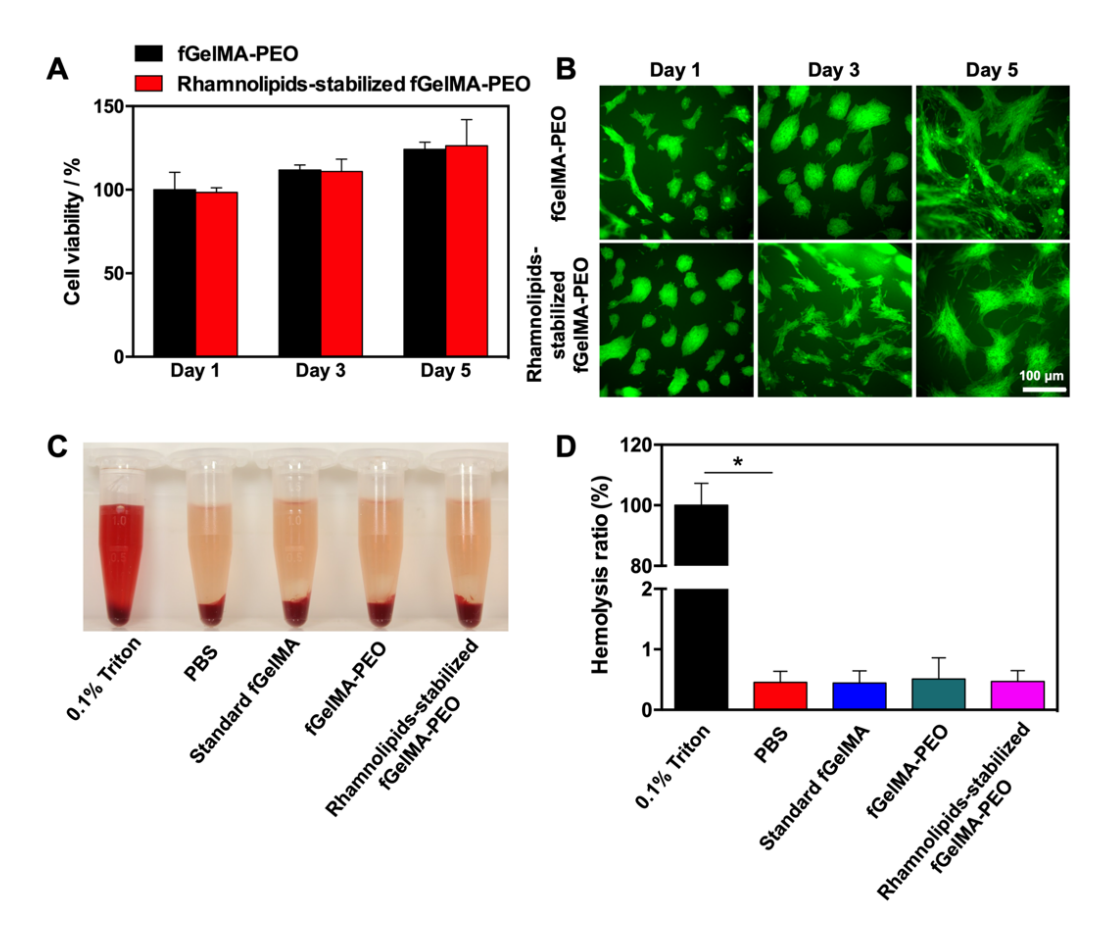


Figure 7. (A) Quantified cytocompatibility evaluation of the fGelMA-PEO and rhamnolipids-stabilized fGelMA-PEO inks by contact-culture with HUVECs. (B) Morphology of HUVECs after culturing on constructs printed from fGelMA-PEO and rhamnolipids-stabilized fGelMA-PEO inks on 1, 3, and 5 days. (C) Photograph showing hemolytic activities of the standard fGelMA, fGelMA-PEO, and rhamnolipids-stabilized fGelMA-PEO inks. (D) Quantified hemolytic percentages for the standard fGelMA, fGelMA-PEO, and rhamnolipids-stabilized fGelMA-PEO inks.

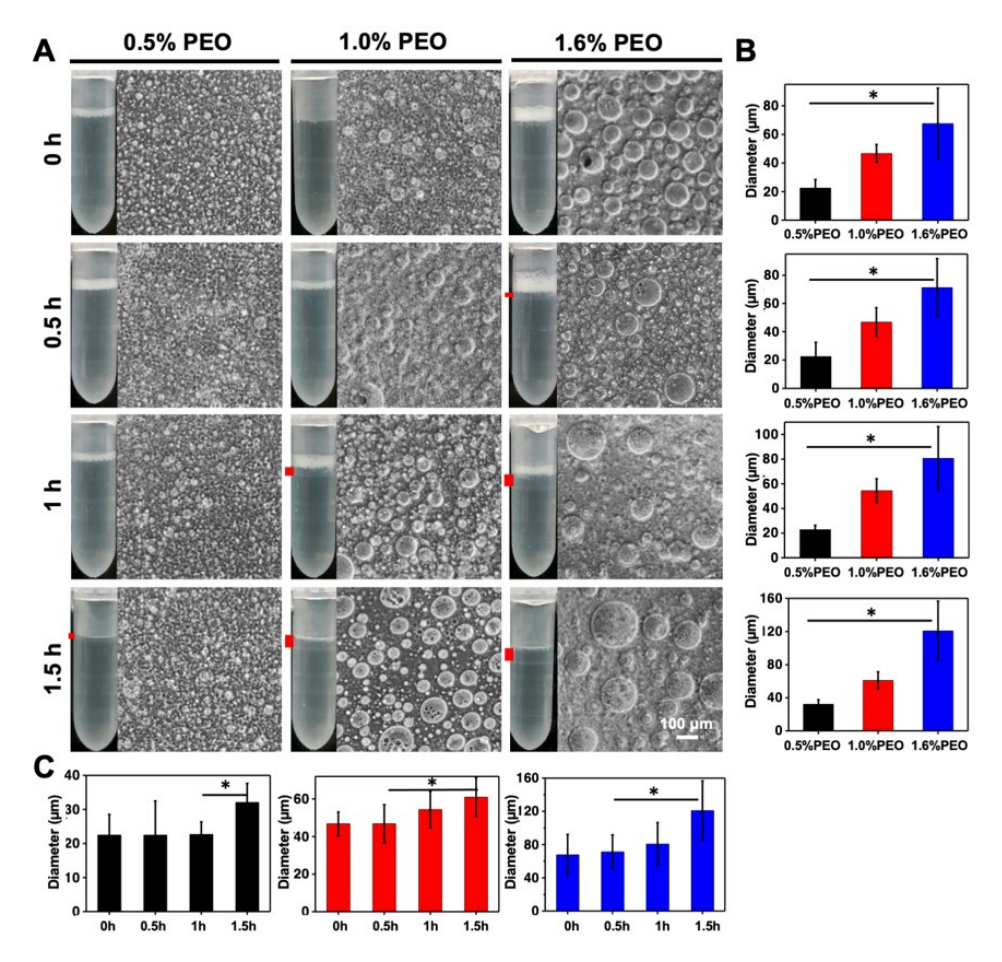


Figure S1. Characterizations of the pGelMA-PEO micropore-forming inks. (A) Optical micrographs showing the pGelMA-PEO inks with different PEO concentrations (0.5, 1.0, 1.6% w/v) and different storage times (0-1.5 h) at room temperature. Red bars indicate the phase-segregation heights of the emulsions in the inks over time. (B) Quantification showing the average sizes of the PEO emulsion droplets of the pGelMA-PEO inks at each time point as a function of different PEO concentrations (0.5, 1.0, 1.6% w/v). (C) Quantification showing the average sizes of the PEO emulsion droplets of the pGelMA-PEO inks at each PEO concentration as a function of different storage times (0-1.5 h) at room temperature.

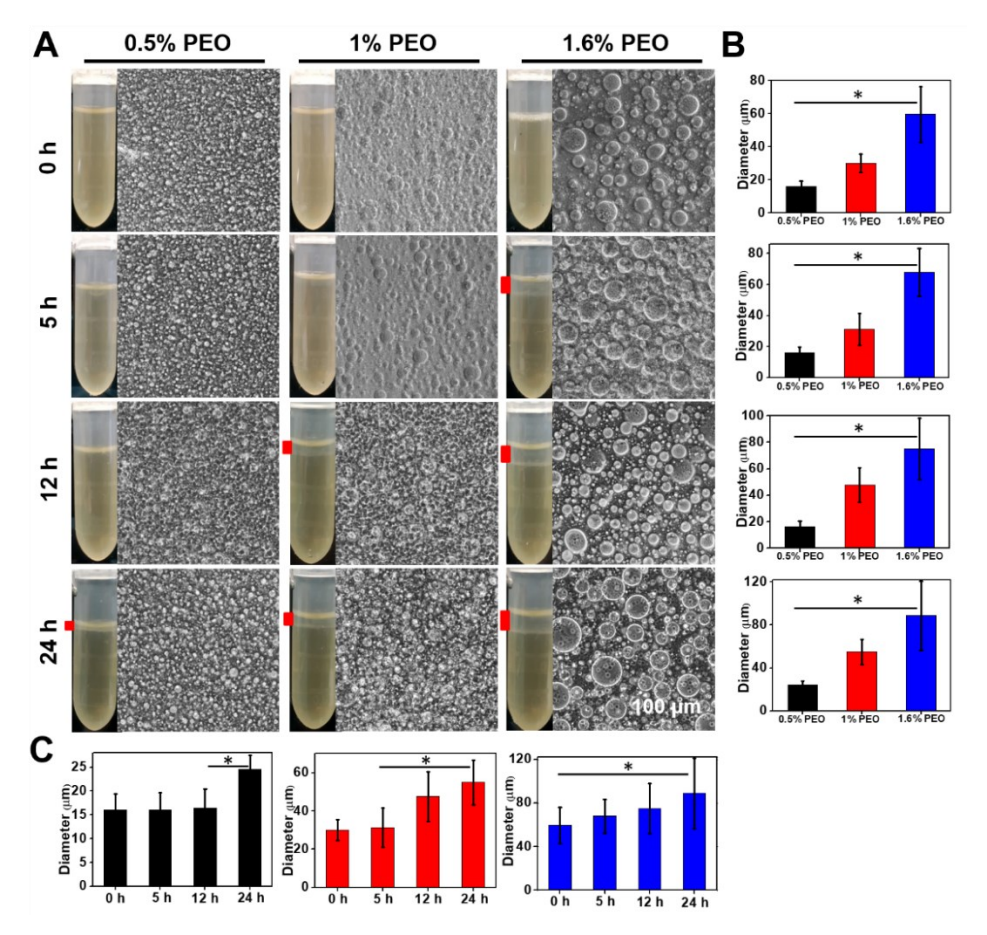


Figure S2. Characterizations of the pGelMA-PEO micropore-forming inks with 1.5% w/v rhamnolipids. (A) Optical micrographs showing the rhamnolipids-stabilized pGelMA-PEO inks with different PEO concentrations (0.5, 1.0, and 1.6% w/v) and different storage time (0-24 h) at room temperature. Red bars indicate the phase-segregation heights of the emulsions in the inks over time. (B) Quantification showing the average sizes of the PEO emulsion droplets of rhamnolipids-stabilized pGelMA-PEO inks with different PEO concentrations (0.5, 1.0, and 1.6% w/v). (C) Quantification showing the average sizes of the PEO emulsion droplets of the rhamnolipids-stabilized pGelMA-PEO inks at each PEO concentration as a function of different storage times (0-24 h) at room temperature.

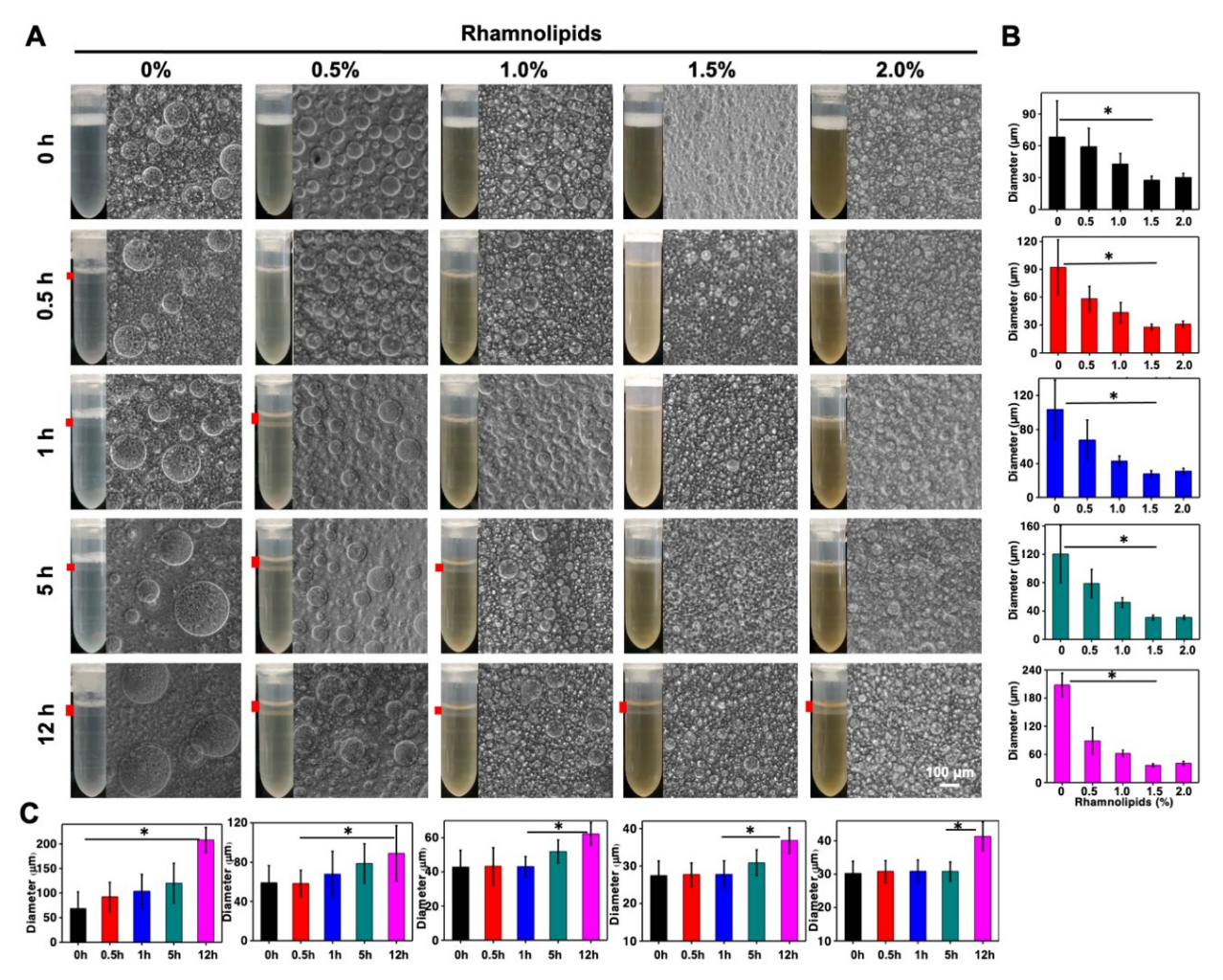


Figure S3. The influence of rhamnolipids concentrations on the pGelMA-PEO micropore-forming ink-formation and stabilization. (A) Optical micrographs showing pGelMA-PEO inks at 1.0% w/v PEO concentration with different rhamnolipids concentrations (0, 0.5, 1.0, 1.5, and 2.0% w/v) and different storage times (0-12 h) at room temperature. Red bars indicate the phase-segregation heights of the emulsions in the inks over time. (B) Quantification showing the average sizes of the PEO emulsion droplets of the pGelMA-PEO inks at 1.0% w/v PEO concentration with different rhamnolipids concentrations (0, 0.5, 1.0, 1.5, and 2.0% w/v). (C) Quantification showing the average sizes of the PEO emulsion droplets of the rhamnolipids-stabilized pGelMA-PEO inks at each rhamnolipids concentration as a function of different storage times (0-12 h) at room temperature.

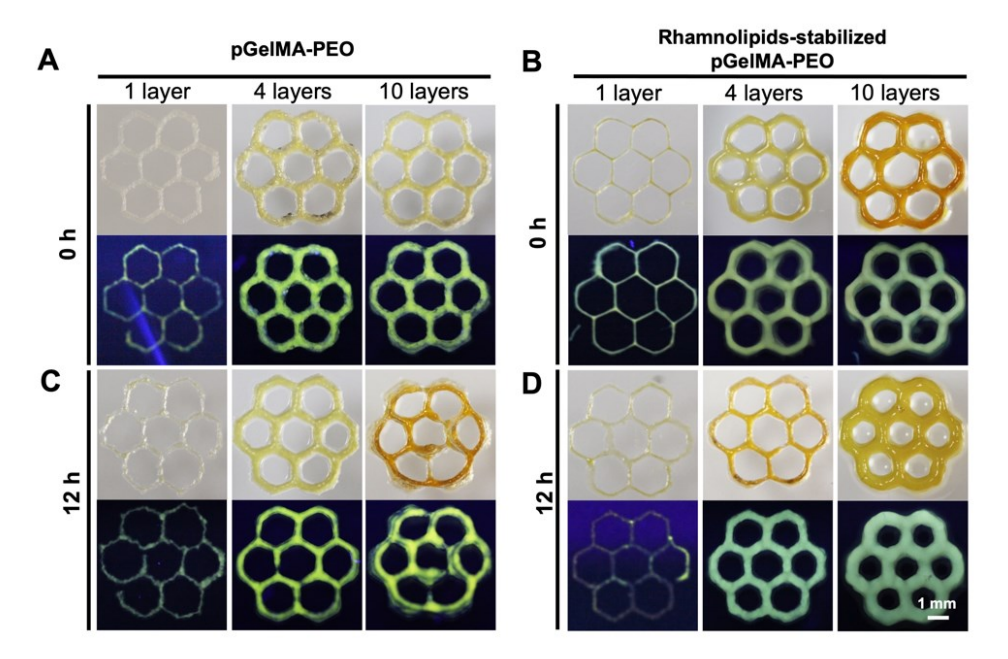


Figure S4. Extrusion printing of the pGelMA-PEO micropore-forming inks. Regular and fluorescence photographs showing top views of 3D constructs printed from (A) fresh pGelMA-PEO ink and (B) rhamnolipids-stabilized pGelMA-PEO ink, as well as (C, D) 3D constructs printed with the same formulations stored at room temperature for 12 h, all under top view.